A. Capannolo, F. Ferrari, M. Lavagna
Families of Bounded Orbits Near Binary Asteroid 65803 Didymos
Journal of Guidance Control and Dynamics, Vol. 42, N. 1, 2019, p. 189-198
doi:10.2514/1.G003437

Families of bounded orbits near binary asteroid 65803 Didymos

Andrea Capannolo*, Fabio Ferrari† and Michèle Lavagna‡
Politecnico di Milano, Via La Masa 34, 20156, Milano, IT

Nomenclature

a, b, c	=	Semi-axes of ellipsoid $[m]$
$C_{0,1}$	=	Jacobi constant for point mass and modified gravitational fields
dE	=	Jacobi constants difference
$\mathbf{F}$	=	Vector of objective functions
G	=	Gravitational constant $[\frac{m^3}{kgs^2}]$
$\underline{\underline{J}}$	=	Jacobian matrix
$U_{ell,poly}$	=	Ellipsoid/Polyhedron gravitational potential $[\frac{m^2}{s^2}]$
$\tilde{U}_{ell,poly}$	=	Nondimensional Ellipsoid/Polyhedron gravitational potential
$\mathbf{X}$	=	Vector of free variables
ρ	=	Mean density $[\frac{kg}{m^3}]$

I. Introduction

Orbital dynamics around complex-shaped bodies is a topic of great interest nowadays. Small celestial bodies of the Solar System are the current frontier of space exploration: the accessibility of the Near-Earth Asteroid (NEA) population makes them suitable candidates to pursue the exploration of our Solar System. When dealing with such bodies, a relevant aspect concerns

*Ph.D. Candidate, Department of Aerospace Science and Technology, andrea.capannolo@polimi.it
†Postdoctoral Research Fellow, Department of Aerospace Science and Technology, fabio1.ferrari@polimi.it, AIAA Member.
‡Associate Professor, Department of Aerospace Science and Technology, michelle.lavagna@polimi.it, AIAA Member.

trajectory design of spacecraft orbiting them. Due to their peculiar properties, asteroids possess a very weak and irregular gravity field. The dynamics of a spacecraft in the close proximity of these bodies are subjected to an extremely chaotic behavior, which makes the design of orbits and trajectories very challenging.

In the last few decades and years, some effort has been made to develop models suitable to accurately reproduce the gravity field around small and irregular celestial bodies. These methods replaced the classical central field Keplerian model, which is not suitable to accurately represent the mass distribution of such complex bodies. Popular methods include shape-based techniques and mass-concentrated models. Shape-based methods are used to model the celestial body as an object with specific shape, such as ellipsoids [1] or polyhedra [2, 3]. The distribution of mass depends on the shape of the body, and it is usually considered homogeneous. Non-homogeneities among the body are usually modeled using mass-concentrated (mascon) models. The mascon method was first developed to explain the anomalies of the Moon's gravity field [4] and helped in the development of a highly accurate lunar gravity model. A similar technique is used to reproduce the gravity field of asteroids [5–7]. The designer's choice on the method to be used depends on the information available on the body's mass distribution and on the level of accuracy required. Typically, each model fits a specific class of asteroids and application range.

These enhanced models of the gravity field around small celestial bodies are used to study and generate trajectories under a more accurate and realistic dynamics. Relevant studies and examples include the generation of orbits close to asteroids 4179 Toutatis [3], 433 Eros [8] and 216 Kleopatra [9]. The paper specifically investigates periodic motion about a binary asteroid system. Relevant results regarding binary asteroids include the work by [10–13].

This work shows families of periodic orbits in the close proximity of binary asteroid 65803 Didymos (main system's characteristics are reported in [14]). Didymos is the target body of the Asteroid Impact and Deflection Assessment (AIDA) [15], a joint cooperation between NASA [16] and ESA [17]. Few results have been published in the past few years regarding the dynamical environment of Didymos, mainly about landing opportunities for the MASCOT-2 (Mobile Asteroid

Surface Scout-2) spacecraft, to be released on the smaller asteroid of the couple, informally called "Didymoon" [18, 19]. Most published studies assume spherical and ellipsoidal shaped attractors [13, 20, 21], or assume multiple, rigidly connected, point masses [10]. Studies exploting the real shape of the asteroids are, on the other hand, limited in terms of number of studied orbits, which have been selected for specific missions purposes [21]. The novelty of this paper is twofold. Firstly, various set of orbits around Lagrangian points are generated with a high-fidelity asteroid model, to study the local effects of perturbed gravitational field with respect to an equivalent point mass system. Secondly, a novel method for orbit generation, based on attractors' shape continuation, is exploited. To compare orbital families in the two models, a synchronous system (with axisymmetric primary and tidally locked secondary) is initially assumed, to provide insight on the effect of the uneven mass distribution, while averaging periodic disturbances that arise from primary asteroid rotation. Successively, exact shape and rotation of the primary are introduced to assess robustness of stable orbits in the non-synchronous system.

II. Didymos dynamical system

The dynamics of the problem are modeled using a Shape-based Circular Restricted Three-Body Problem (also referenced here as SCR3BP). The model is based on the classical Circular Restricted Three-Body Problem (CR3BP) formulation, but it makes use of shape-based models to reproduce the gravity field of primaries. Nonetheless, the motion of primaries still relies on Keplerian dynamics (as for CR3BP), and it is not affected by their non-spherical mass distribution. Consequently, the distance of primaries is constant in time as they move with constant velocity on a circular path around the barycenter of the system. Initially, the rotational motion of the two asteroids is synchronized with their orbital period: the primary attractor shape is averaged around the spin axis (orthogonal to the orbital plane), while the secondary attractor is assumed to be tidally locked to the primary. Under these assumptions, the relative rotation between the two asteroids is null, thus making the dynamical problem autonomous, since it does not depend explicitly on time. As a consequence, it is possible to define periodic orbits that do not depend on the initial attitude of the attractors,and approximate the

real non-periodic motion arising from asteroids' rotations. Successively, the primary's exact shape and rotation are restored to assess the effect of the gravitational oscillation on the periodic orbits found in the averaged asteroid model. The nondimensional equations of motion of the spacecraft in the synodic frame (co-rotating with primaries) are very similar to that of CR3BP:

$$\begin{cases} \ddot{x} = x + 2\dot{y} + \tilde{U}_{\text{poly}_x} + \tilde{U}_{\text{ell}_x} \\ \ddot{y} = y - 2\dot{x} + \tilde{U}_{\text{poly}_y} + \tilde{U}_{\text{ell}_y} \\ \ddot{z} = \tilde{U}_{\text{poly}_z} + \tilde{U}_{\text{ell}_z} \end{cases} \tag{1}$$

where x, y, z represent the position in the synodic frame, the subscript $(\cdot)_x$, $(\cdot)_y$ or $(\cdot)_z$ indicate partial derivatives, and $\dot{(\cdot)}$, $\ddot{(\cdot)}$ are the time derivatives. As discussed, the difference between Eq. (1) and the equations of motion of the CR3BP is to be found in the gravity potential of primary sources ($\tilde{U}_{\text{poly}}$ and $\tilde{U}_{\text{ell}}$). According to the latest observations of Didymos system, information on the shape of the asteroids are partially available. The mass distrubution of the primary asteroid (also called "Didymain") is modeled using its polyhedral shape model*, while Didymoon's shape is estimated to be an elongated tri-axial ellipsoid. Accordingly, $\tilde{U}_{\text{poly}}$ and $\tilde{U}_{\text{ell}}$ represent the nondimensional gravitational potential due to Didymain and Didymoon.

The expression of the primary's potential, modeled as a constant density polyhedron, is based on the method proposed by Werner and Scheeres [2]:

$$U_{\text{poly}}(x, y, z) = -\frac{1}{2} G\rho \left(\sum_{f \in \text{faces}} \boldsymbol{r}_f \cdot \mathbf{F}_f \cdot \boldsymbol{r}_f \omega_f - \sum_{e \in \text{edges}} \boldsymbol{r}_e \cdot \mathbf{E}_e \cdot \boldsymbol{r}_e L_e \right) \tag{2}$$

where $\mathbf{F}_f$ is the dyad associated to face f and $\mathbf{E}_e$ is the dyad associated to edge e of the polyhedron model, L_e represents the potential of a wire associated to the edge e, and ω_f is the solid angle associated to the face f. The expression of the aforementioned quantities is described in [2]. The

*The Didymain shape model is used in the frame of the AIM contract, however it is still unpublished (courtesy of L. Benner and S. Naidu)

secondary's potential, modeled as a constant density tri-axial ellipsoid, is derived in [22]:

$$
\begin{aligned}
U_{\text{ell}} = & \frac{2G\rho\pi abc}{\sqrt{a^2-c^2}} \left\{ \left[1 - \frac{x^2}{a^2-b^2} + \frac{y^2}{a^2-b^2} \right] F(\omega_\kappa, k) + \right. \\
& + \left[\frac{x^2}{a^2-b^2} - \frac{(a^2-c^2)y^2}{(a^2-b^2)(b^2-c^2)} + \frac{z^2}{b^2-c^2} \right] E(\omega_\kappa, k) + \\
& \left. + \left[\frac{(c^2+\kappa)y^2}{b^2-c^2} - \frac{(b^2+\kappa)z^2}{b^2-c^2} \right] \frac{\sqrt{a^2-c^2}}{\sqrt{(a^2+\kappa)(b^2+\kappa)(c^2+\kappa)}} \right\}
\end{aligned} \tag{3}
$$

where $a > b > c$ are the semi-axes of the ellipsoid, F and E are the Legendre's elliptic integrals of first and second kind, and κ is the largest root of a cubic expression, defined in [22].

III. Numerical method

The unpredictable local variations in the gravitational field due to uneven mass distribution, and the higher computational cost deriving from high fidelity polyhedral model, suggest a lighter approach for orbital families generation than the classical one in use for the CR3BP [23–25]. The strategy is subdivided into "initialization", "correction" and "continuation" phases. These are discussed in detail in the following sections.

A. Initialization

The initialization phase exploits already known families from CR3BP through a sampling process: for each family, a subset of evenly spaced orbits is selected and saved for next steps of the orbit generation process. The reduced number of orbits allows lower computational cost, while their uniform distribution preserve the overall trends of size, period and stability, along the entire family.

B. Continuation

The continuation step acts on the gravitational field rather than on the orbits: fixing the sampled trajectory, a modification of the attractors's shape is introduced through a parameter α, which turns the bodies from spheres (when $\alpha = 0$) to the real shape (when $\alpha = 1$). The gradual modification of α allows smooth variation of the gravity field from the spherical model (equivalent to point mass)

to the asteroids model. The irregularly shaped bodies possess a surface point with the minimum distance from the center of mass, being it the radius of the inscribed sphere of the object. The difference between the radius at each surface point of the body and the radius of the inscribed sphere can be scaled using α and added to the inscribed sphere to introduce irregularities. The system to be solved reads:

$$\begin{cases} r_S = \min(\mathbf{r_B}) \\ \mathbf{r}_\alpha = r_S[1 + \alpha(\frac{\mathbf{r_B}}{r_S} - 1)] \end{cases} \tag{4}$$

with $\mathbf{r_B}$, r_S and $\mathbf{r}_\alpha$ being respectively the vector of all distances of surface points from the center of mass, the radius of the inscribed sphere, and the vector of the scaled surface's points distances from center. It is worth underlining that, in order to go from the spherical model to the actual shape model of the body without changing the mass ratio between attractors, the homogeneous density of the bodies shall be adjusted according to the volumes update at each step.

C. Correction

The perturbations on the gravity field, introduced by the continuation, will distort the orbit, making it lose its periodicity. To restore it, a shooting algorithm (as the one adopted for CR3BP) is used [25], with extension to a multi-nodal scheme to deal with the increased sensitivity of the problem. The trajectory is divided into many nodes equally spaced in time (3 per nondimensional time unit). The purpose of the correction scheme is to nullify the difference between the state of each node and the propagated state from the previous node, in order to have a continuous trajectory either in position and velocity. Periodicity is ensured through an additional continuity constraint between initial and final node. A tolerance is set to assess whether the target periodic orbit has been reached. To implement correction of the trajectory, a damped method (Levenberg-Marquardt) is used, to avoid overshooting issues arising from the strong sensitivity of the problem. The numerical scheme equation reads:

$$\partial \mathbf{X} = -\left(\underline{\underline{J}}^T \underline{\underline{J}} + \lambda \cdot diag(\underline{\underline{J}}^T \underline{\underline{J}})\right)^{-1} \underline{\underline{J}}^T \mathbf{F} \tag{5}$$

being λ the damping parameter. As mentioned, the constraints vector contains conditions to enforce continuity (difference between the i-th nodes' state and propagated state from the $(i-1)$-th nodes: $6(N-1)$ conditions) and periodicity (continuity between final and initial node: 6 conditions). Overall, the length of the constraint vector is $6N$. The presence of a variable period requires an additional constraint to solve problem: the total number of free variables is $6N+1$ (N state at nodes plus period). The $(N+1)$-th condition is provided through the conservation of the Jacobi constant, allowing also to generate families with specific energy levels in both models, for a more meaningful comparative analysis. The conservation of Jacobi constant is ensured through Eq. (6):

$$\begin{cases} C_i = 2\Big(U(x_i, y_i, z_i) - \frac{1}{2}(\dot{x}_i^2 + \dot{y}_i^2 + \dot{z}_i^2)\Big) \quad , \quad i = 0, 1 \\ dE = C_1 - C_0 \end{cases} \tag{6}$$

Although the formulated problem provides a unique orbit, the nodes are not yet constrained and may move along the trajectory. To avoid such phenomenon, the y position of the initial node (y_1^n) is constrained to its initial value "y_0". The final constraint vector reads:

$$\mathbf{F} = \left\{ \mathbf{x}_2^p - \mathbf{x}_2^n; \quad \mathbf{x}_3^p - \mathbf{x}_3^n; \quad \dots \quad \mathbf{x}_N^n - \mathbf{x}_1^n; \quad dE; \quad y_1^n - y_0 \right\}^{\mathrm{T}} \tag{7}$$

with $\mathbf{x}_i^p$ and $\mathbf{x}_i^n$ being respectively the propagated state from (i - 1)-th node and the state of i-th node. The term $\mathbf{x}_N^n - \mathbf{x}_1^n$ is the periodicity condition. Coherently, the Jabobian matrix is expressed as:

$$\underline{\underline{J}} = \begin{bmatrix} \frac{\partial \mathbf{x}_2^p}{\partial \mathbf{x}_1^n} & -\mathbf{I}_6 & & & \frac{\dot{\mathbf{x}}_2^p}{N-1} \\ & \ddots & \ddots & & \vdots \\ & & \frac{\partial \mathbf{x}_N^p}{\partial \mathbf{x}_{N-1}^n} & -\mathbf{I}_6 & \frac{\dot{\mathbf{x}}_N^p}{N-1} \\ -\mathbf{I}_6 & & & \mathbf{I}_6 & \mathbf{0}_6 \\ \frac{\partial dE}{\partial \mathbf{x}_1^n} & & \dots & \frac{\partial dE}{\partial \mathbf{x}_N^n} & \mathbf{0}_{(1\times 6)} \\ \frac{\partial y_1^n}{\partial \mathbf{x}_1^n} & \mathbf{0}_{(1\times 6)} & \dots & & \mathbf{0}_{(1\times 6)} \end{bmatrix} \tag{8}$$

where the last column is related to the variable period, the last eight rows are respectively the connection of initial and final state (from first to sixth row), the energy constraint (seventh row), and the initial node "y" constraint (eighth row), while the upper left block is the sparse matrix ensuring the connection of all nodes. At each iteration the algorithm reduces the parameter λ (if converging), or increases it (if diverging), consequently making the corrector move towards a Newton method or a steepest descent method [26] . The residual evaluated to assess the convergence is defined as:

$$r = \|\mathbf{F}\| \tag{9}$$

To modify the parameter λ, a direct correlation with the residual is adopted, such that $\lambda = \xi\, r^2$, which speeds up the process [27]. Acting on "ξ", the damping term can be adjusted. The overall procedure stops when continuity and periodicity are ensured within tolerances, and final shape of the attractors is obtained.

IV. Periodic orbits in the SCR3BP

The selection of the orbits to be analyzed has been driven by their effectiveness in the framework of the Asteroid Impact Mission design. Four different families are studied in the CR3BP environment:

- Distant Retrograde Orbits (DRO)
- Short Period Orbits (SPO) around L4
- Halo Northern/Southern Orbits around L1 and L2 (HNL1/HSL1/HNL2/HSL2)
- Lyapunov Orbits around L1 and L2 (LyL1/LyL2)

The properties of these families are studied and compared in the two different models of dynamics (point masses and asteroids), highlighting differences in terms of period, shape, size and stability. Each orbit is identified with a Jacobi constant, defining its position along the family and, also giving an idea of the size with respect to the rest of the family. In particular, as the distance of the orbit from its reference equilibrium point increases, orbital size increases as well. At the same time, it is observed, for all the families under study, a reduction of the Jacobi constant. For this reason, when

studying orbital properties with respect to increasing size, the graphs shall be looked at from highest C_0 to lowest, that is, from the right side to the left side of plots.

After a visual representation of families in the "Point Mass" and "Asteroids" models, the analysis of the most relevant features of each family is illustrated, highlighting the main differences between the models used.

A. DRO (Distant Retrograde Orbits)

DRO are characterized by a wide span of sizes, from very small orbits (close to the secondary attractor) to very large ones (close passages to main attractor), thus being suitable for very different applications. The natural stability characterizing these orbits represents a further advantage that extends their exploitation to spacecraft with very cheap station keeping control expense.

The comparison between the classical DRO family and the modified version in the shape-based model highlights relevant changes, particularly related to the shape of the orbits. As can be noticed from Fig. 1, the typical planarity of the family is lost and an out-of-plane component is observed. In particular, the out-of-plane component appears to move downwards far from the main attractor, and upwards close to it. Looking at the mean "Z" component and at the vertical oscillations span, as illustrated in Fig. 2(a), two observations arise:

- The vertical mean deviation is roughly proportional to orbital size (that is, to the inverse of Jacobi constant) up to very small orbits.
- The mean deviation value is closer to the lower limit of the "Z" range covered along the orbit.

As a consequence, the majority of orbital period is spent below the plane of the three-body binary system. This is due to the non-symmetric distribution of mass between the northern and southern hemisphere of the primary asteroid. The vertical motion is surely the most relevant and evident effect. In addition, "X" and "Y" components are slightly shrunk for bigger orbits, resulting in overall reduced orbital size (expressed in terms of line integral along the orbit), while small orbits display larger values. In particular, the shrinkage effect relevantly affects orbits closer to main attractor, while the enlargement on the orbital plane is mostly present in small-medium size orbits. (see

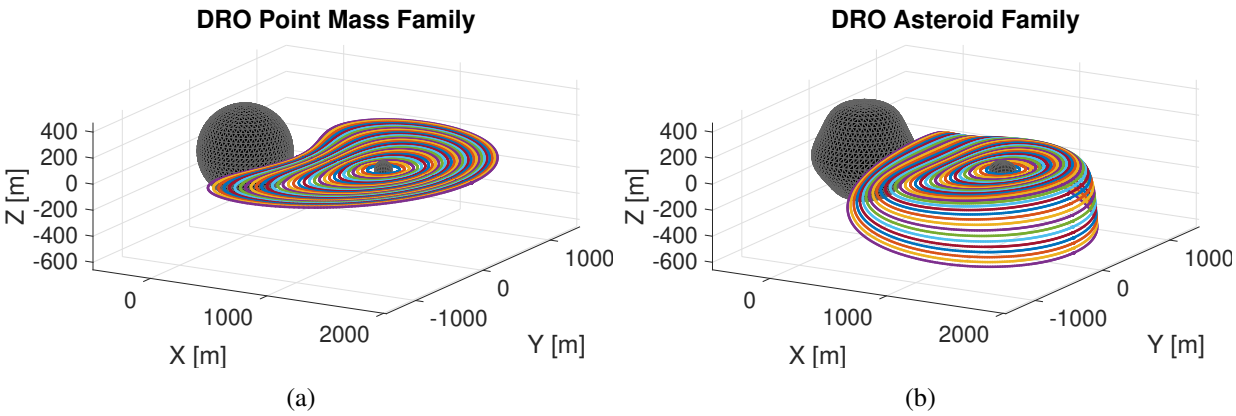

(a) (b)

Fig. 1 DRO family in (a) point mass model and (b) asteroids model

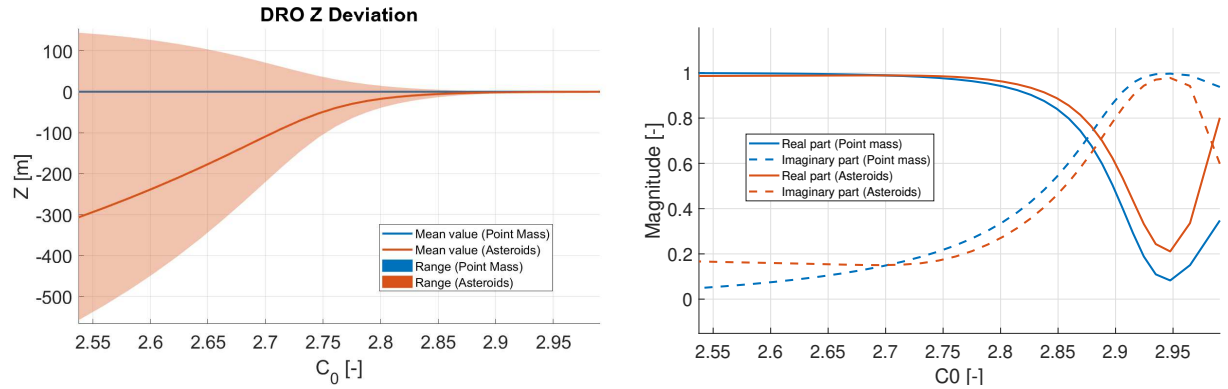

(a) (b)

Fig. 2 DRO family (a) out-of-plane deviation and (b) eigenvalue tracking

Fig. 3(a)). Nevertheless, the size change never goes beyond the 10% of the "point mass" orbit. In the same way, a (negligible) reduction of the orbital period is measured for orbits that are closer to the main attractor, while the smallest (close to secondary attractor "Didymoon") have longer periods, as shown in Fig. 3(b): their period changes up to a maximum around 10%, compared to that of the original trajectory, as a consequence of the combined effect of moonlet's elongated body (J2 effect) and prominent equatorial ridge of primary attractor.

Stability properties are not significantly changed, however, some eigenvalues display slightly different values in specific regions of the family. For example, eigenvalues of smaller orbits in the asteroid model are closer to unitary value, while point mass solutions have values closer to the real axis when moving towards the biggest orbits, as shown in Fig. 2(b).

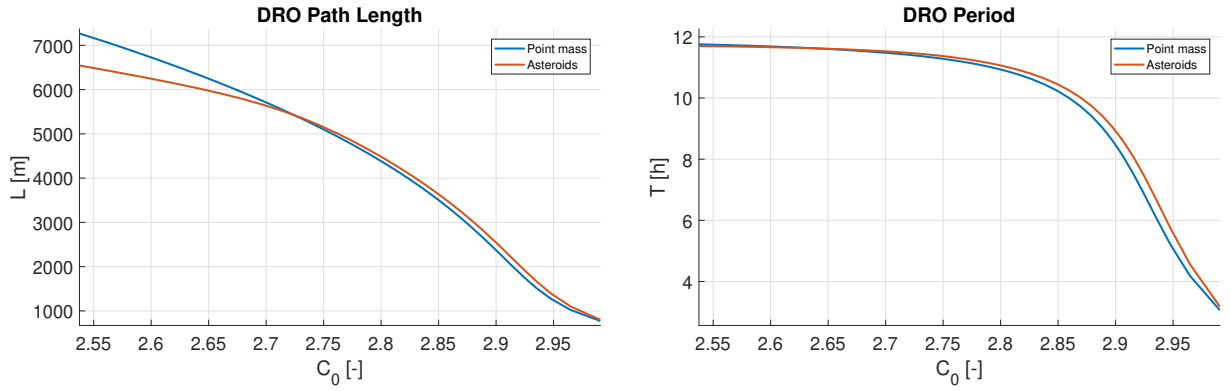

(a) (b)

Fig. 3 DRO family (a) line integral and (b) periods in point mass and asteroids models

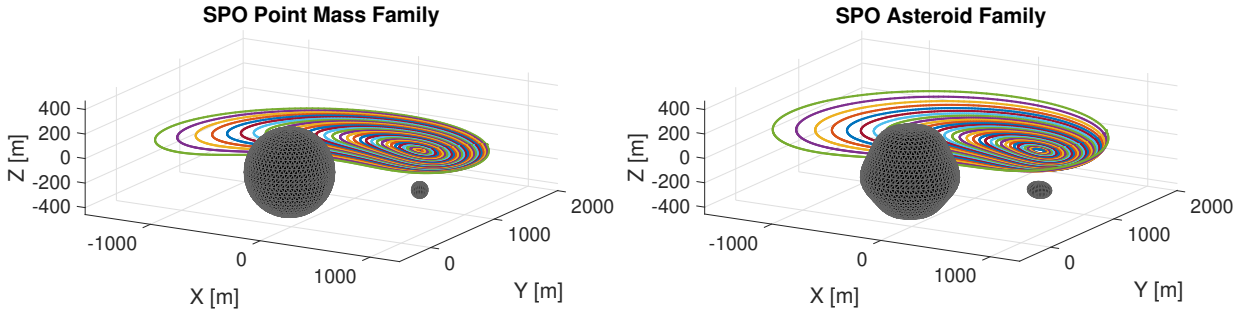

(a) (b)

Fig. 4 SPO family in point mass model (a) and asteroids model (b)

B. SPO (Short Period Orbits)

SPO are located in a stable region of the three-body domain, since they are correlated to libration point L4 and L5. Compared to DRO, they show an opposite size-period behavior: larger orbits have lower periods, so that the spacecraft would move to many positions in the system in a relatively low time. For the case of asteroid exploration missions, this could be particularly advantageous e.g. for gravimetric measurements.

The visual representation of the SPO family in both models (Fig. 4) does not make relevant differences stand out, as observed in the case of DROs. Nonetheless, few conclusions can be drawn. Figure 5(a) shows that a vertical component arises, especially for bigger orbits. In this case, the shift follows a positive Z trend, with time-averaged mean value closer to the upper bound, meaning a longer time spent on the upper region of the binary system plane. In opposition to the DRO case, the

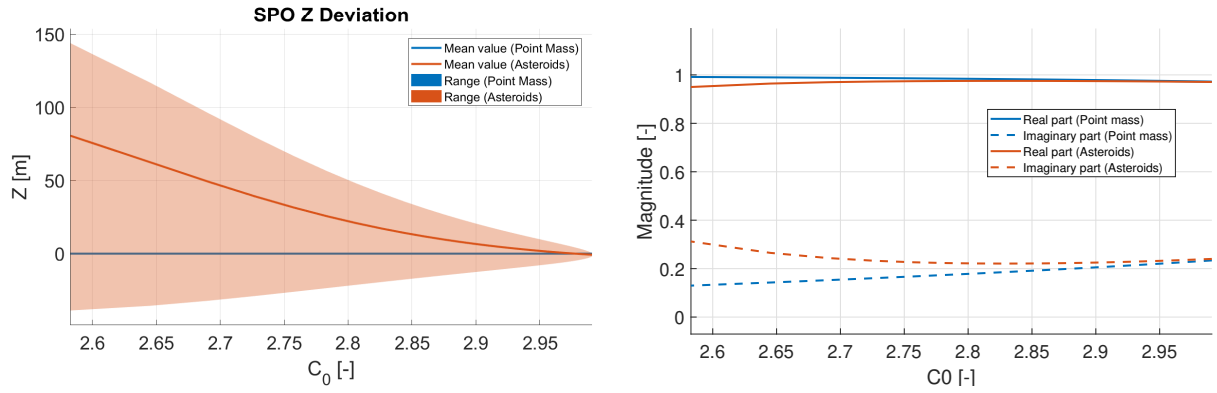

(a) (b)

Fig. 5 SPO family (a) out-of-plane deviation and (b) eigenvalue tracking

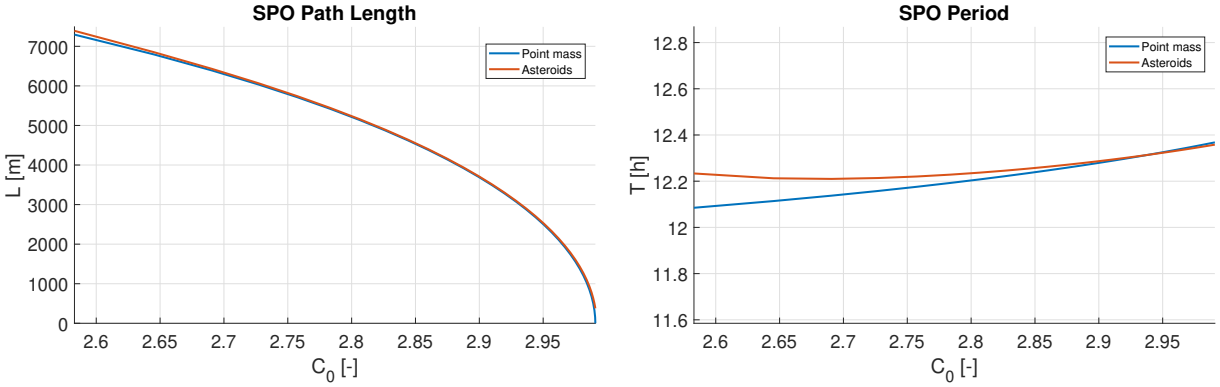

(a) (b)

Fig. 6 SPO family (a) line integral and (b) period in point mass and in asteroids models

farther from the main attractor, the higher the Z component, suggesting a different local influence of the asteroid's mass distribution. The vertical shift is nearly ineffective on the overall orbital size, as illustrated in Fig. 6(a). In fact, bigger orbits are far closer in length to their corresponding in point mass model than smaller ones. The length change of the small trajectories can be explained considering that Jacobi constant of lagrangian points has slightly increased when passing from point mass to asteroids model. The correction method forces conservation of energy and finds the new solution farther from the equilibrium point. This behavior is observed for all other families studied. Interesting results appear from the comparison of orbital period. The typical monotonic trend is replaced by a quadratic-like curve, with the minimum located in the region of largest orbits (Fig. 6(b)), possibly due to the additional vertical component. The eigenvalues show an interesting

behavior along the family. While solutions in the point mass model exhibit a monotonic behavior (with eigenvalue approaching the real axis as orbital size increases), solutions in the asteroid models are not monotonic. In fact, as observed in Fig. 5(b), eigenvalues of smaller orbits share a nearly identical trend between the two models. The trend becomes different from the middle-sized orbits region on.

C. Halo Orbits

Halo orbits are characterized by an out-of-plane motion near secondary attractor [28]. As known, they are intrinsically unstable and require station keeping to avoid long term escaping trajectories or impacts with surface. The comparison between point mass and asteroids halo orbits is carried on in parallel for all four family groups (Northern/Southern-L1/L2), to underline the main differences related to each subgroup. Graphic results are presented for the L1 Halo families, as L2 families display similar trends, however, specific differences will be discussed in the text (Northern L2 family will be depicted to highlight the similarity with the L1 family). From the analysis of the families, it is observed, for all subgroups, how the modification of the gravitational environment leads to an "empty region" between the first halo, departing from Lyapunov family bifurcation, and the rest of the family (Fig. 7). Similarly to what discussed regarding the increase of energy of equilibrium points, this phenomenon can be attributed to a change in the energy variation from one orbit to another, suggesting a lower rate of change of the Jacobi constant in the empty region.

The size of asteroid families are not uniformly shifted from their originating values: smaller orbits appear greater (as a consequence of the energy-related phenomenon), while bigger orbits are shrunk, as illustrated in Fig. 8. Conversely, the period is uniformly shifted towards lower values (with peaks of reduction around 13-14 % of the initial value), and the trend along the families is nearly unchanged, as illustrated in Fig. 9.

A peculiar behavior is observed through the tracking of one of the monodromy matrix's eigenvalues. The L1 families couple displays a highly asymmetric distribution with respect to the binary orbital plane, which is not present in the L2 families. Looking at Fig. 10), it is noticed that

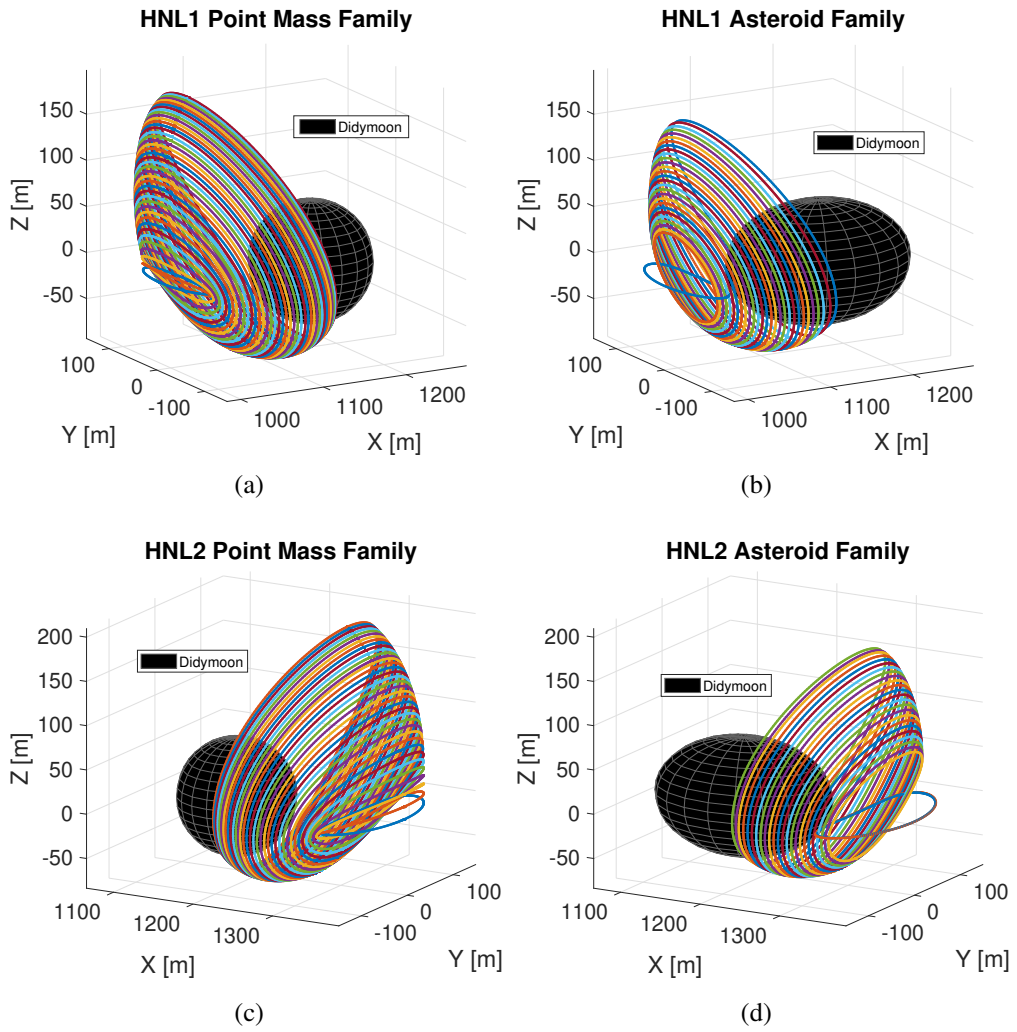

Fig. 7 Northern Halo family around L1 and L2 in point mass model (a,c) and asteroids model (b,d).

Northern L1 family reaches a tangent bifurcation point in (-1;0) of the Real-Complex plane (at some distance from Didymoon), while the same bifurcation is found in Southern L1 family when collision with the asteroid is reached (although a virtual continuation of the family would suggest the same results of the Northern orbits). In contrast, the two families around L2 display comparable trends (close to the one from L1 southern family), being they farther from Didymain, and thus less subjected to the uneven field. It is interesting noting, from all the plots related to Halo families, how asteroid model orbits anticipate every parameter with respect to their point mass counterpart, as they are characterized by higher Jacobi constant values.

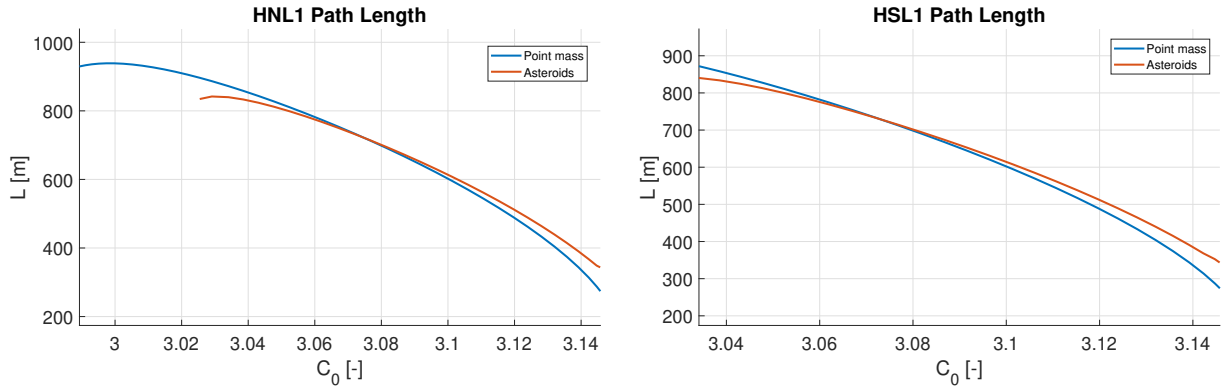

(a) (b)

Fig. 8 Halo families size in point mass and asteroids model. Northern L1 Halo (a) and southern L1 halo (b) are depicted.

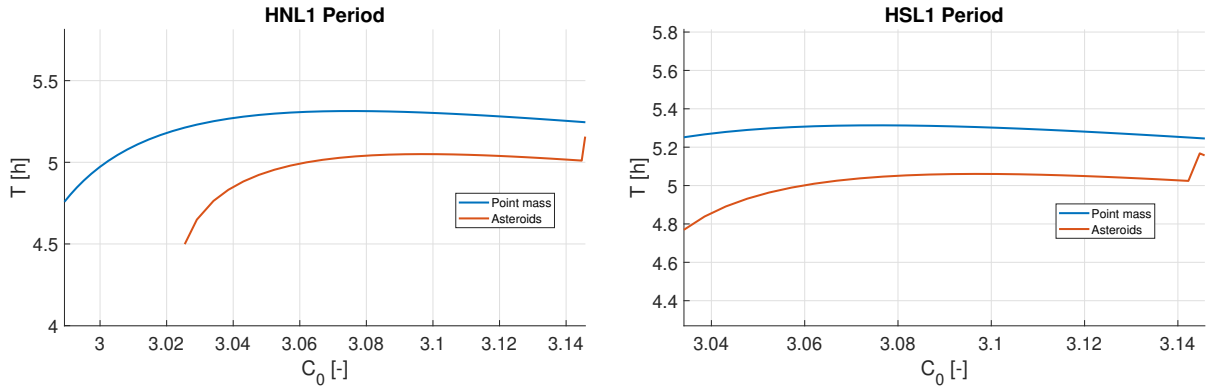

(a) (b)

Fig. 9 Halo L1 family periods in point mass and asteroids model. Northern L1 Halo (a) and southern L1 halo (b) are depicted.

D. Lyapunov Orbits

Lyapunov orbits, as Halo, are characterized by instability and they are close to the secondary attractor. Differently from Halo orbits, they do not possess any out-of-plane component [28]. Together with Halo orbits, they are among the most common orbit families used for mission design and planning.

As for the Halo analysis, plots related to the L1 family are depicted, and differences of the L2 family will be mentioned in the text (as for Halo case, the L2 family is depicted to show the similarity with the L1 family). The comparison between the families in both models, highlights a peculiar

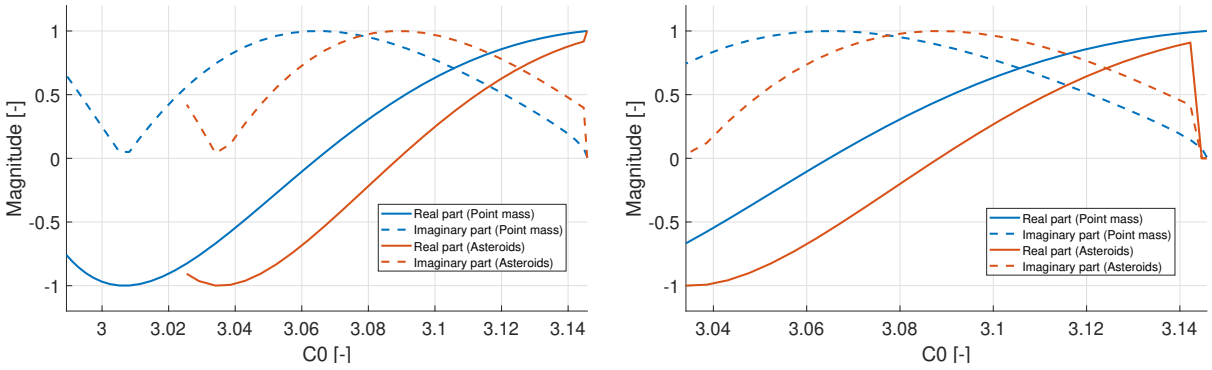

Fig. 10 Halo families eigenvalue tracking. Values for northern L1 Halo (a) and southern L1 halo (b) are depicted.

result of the correction of small Lyapunov orbits in the surroundings of their respective Lagrangian point. In fact, by comparing L1 orbits in Fig. 11, one can observe that small planar Lyapunov orbits are converted into Halo orbits, while keeping the same Jacobi constant (ensured through constraints of the correction algorithm). The shift of energy of the Lagrangian points may cause an increase of the gap between the original Lyapunov and the one having the same Jacobi constant, thus making the process converge towards a closer solution (the Halo orbit). As a consequence, most of parameters of the orbits are subjected to high oscillation for the first orbits, then stabilize while moving away from the equilibrium point.

As for the SPO family, the first orbits of the asteroid model have orbital size significantly higher than their respective in the point mass model, however, the gap shortens as moving towards bigger orbits (quickly reaching a percentage variation below 10%), as shown in Fig. 12(a). It is worth noting that, despite the vertical imbalance of primary's gravity field, the orbits (non degenerating into Halo family) maintain a quasi-planar behavior, with oscillations on the Z axis of the order of few meters. On the contrary, most of the dimensions variation is due to the Y component of the motion, with asteroid model orbits more prominent with respect to Didymoon's sides (Fig. 12(b)).

Regarding orbital period, minor differences have been detected, with deviations from the point mass model lower than 5 %.

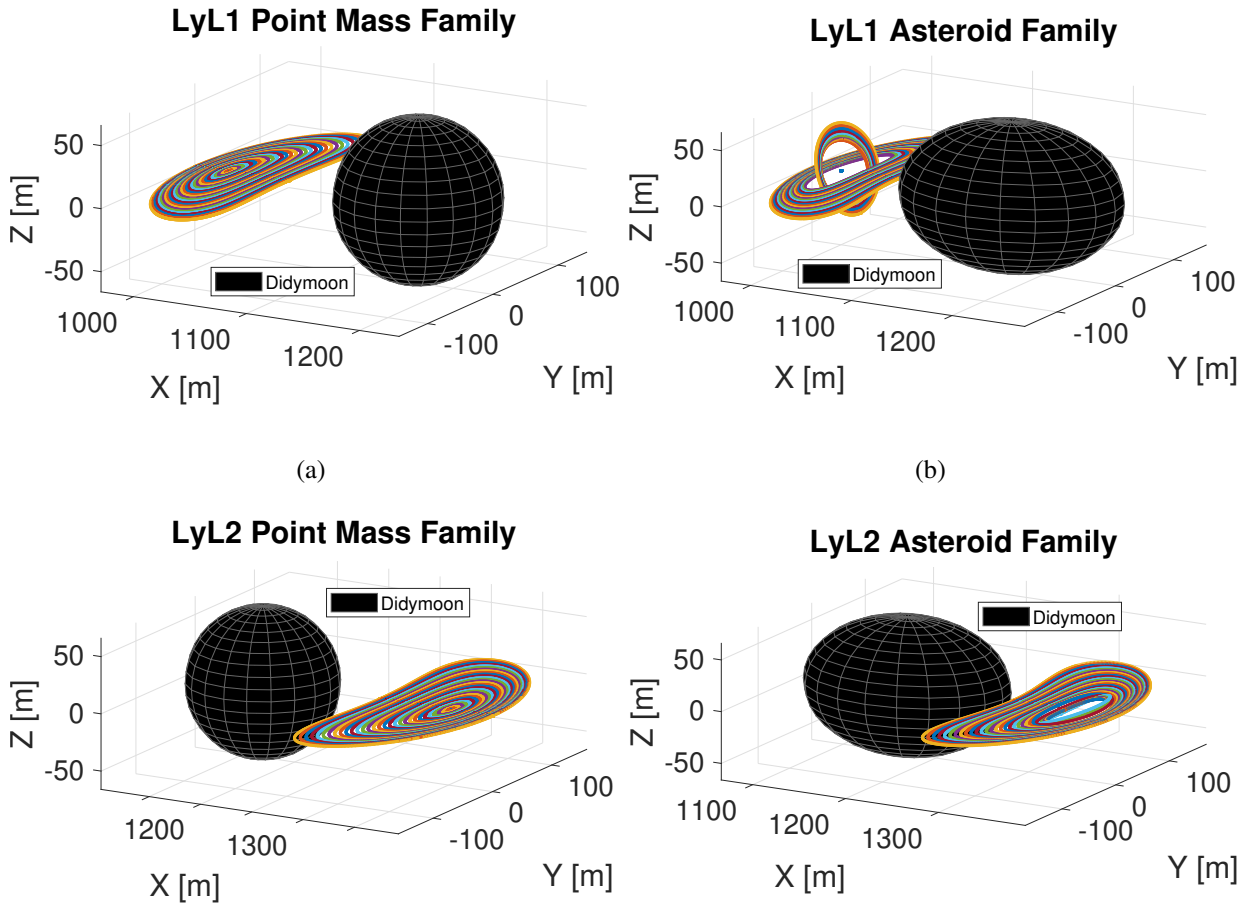

Fig. 11 Lyapunov L1 and L2 family in point mass model (a,c) and asteroids model (b,d).

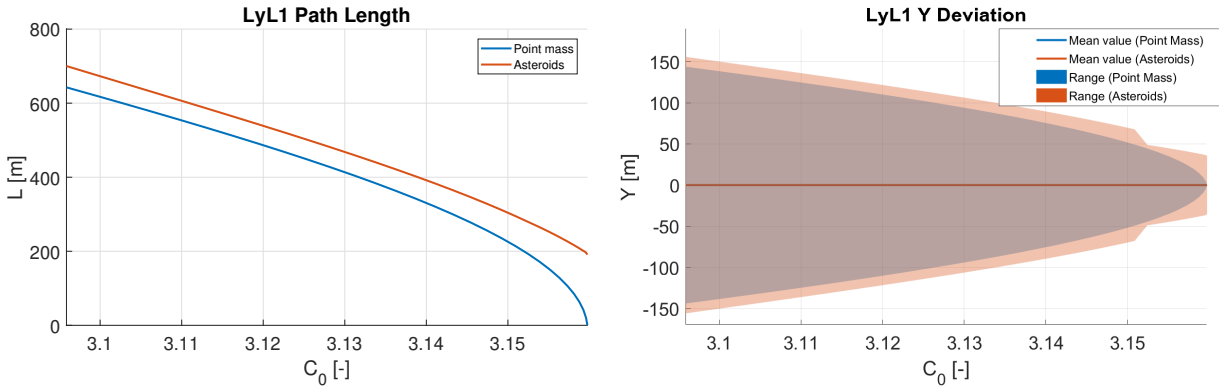

Fig. 12 Lyapunov L1 family (a) line integral and (b) Y deviation in point mass and in asteroid model

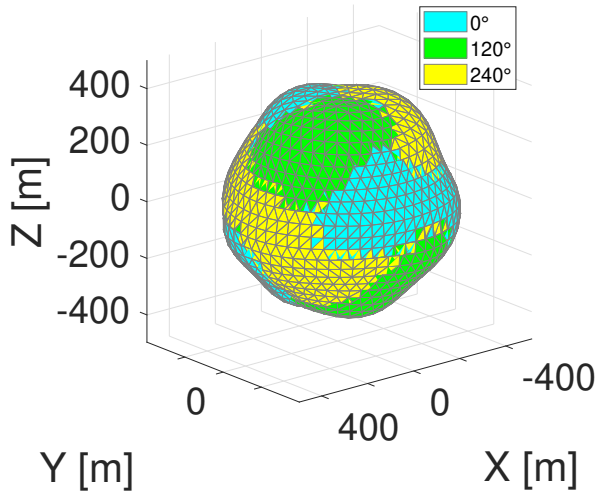

Fig. 13 Didymain attitudes and gravity dominance regions.

V. Sensitivity analysis

The periodic families described in Section IV are obtained through the assumption of an axisymmetric primary, to take into account average effects of its rotation. This reduction of complexity of the model is necessary to provide the sufficient regularity to orbits, to analyze the effects of irregular shapes with respect to spherical masses. As a consequence, the study requires an assessment of the robustness of trajectories in a more realistic environment. Three initial angles for the attitude of the primary (with respect to the spin axis Z) are considered, namely the 0° , the 120° and the 240° configurations. A constant rotation along Z axis is then introduced (accordingly to the rotation period presented in [14]), and initial conditions of the periodic orbits propagated for a time equal to ten times the common multiple of orbital period and asteroid rotation period, given by their product. It is important to underline that only stable periodic orbits have been considered for this analysis, since it is interesting to assess to what extent their stability properties are valid, while an immediate divergence of unstable orbits is expected and no further information would be given.

Figure 13 shows the three attitudes overlapped, to highlight which one is more prominent (and, consequently, more perturbing) in each zone. For sake of clarity, regions aligned with X axis will be named "front-back" areas, those aligned with Y axis "left-right" (left corresponding to positive Y), and those aligned with Z axis "north-south". As can be observed, the front region is dominated by the 240° attitude, with small influence in the north region of 120° attitude and in the south region

of the 0° attitude. Instead, the left region is largely occupied by the 0°, with higher influence of the 120° in the south area and a small presence of the 240° in the north region (shifted towards the left-back area). This unbalance of mass distribution along the north-south direction causes a continuous shift of gravity force in a vertical direction, while the equatorial prominent ridge (with a peak in the front region of the 240° configuration) creates a periodic disturbance in the orbital plane.

This ridge is likely to be the main cause of the instability and divergence that have been observed for all the largest DRO and SPO orbits passing close to the asteroid's surface. This instability is, however, foreseeable if looking at the eigenvalues behavior along the two families (Fig. 2(b) and Fig. 5(b)), where proximity to the real axis is maximized for large orbits.

Exception made for the aforementioned orbits, the study of asteroid's rotation effect is carried on for the smallest DRO and SPO, and for large trajectories of the same families (in particular, the last ones showing some stability property before reaching the complete divergence in the family).

The DRO family is characterized by periods that go from 1:1 to 4:1 ratios with respect to Didymain's rotation, thus having various chances to display resonance phenomena. However, the large variation in dimensions and distances from the main asteroid make the resonance responses different. In fact, considering small DRO, the 1:1 period ratio would suggest relevant perturbing effects, but the proximity to Didymoon introduces more stability, thus leaving the orbits nearly unchanged (oscillations are below one meter). Nevertheless, it is interesting to notice that the initial attitude of the primary asteroid still affects the period of the orbit in a long term fashion, by reducing or increasing it of a small quantity (see the change in phase of the three oscillations in Fig. 14). On the other hand, large DRO orbits, which are close to a 4:1 ratio, are visibly influenced by the rotation, with different behavior as the initial asteroid's attitude changes (Fig. 15). In particular, mean position's oscillations are of the order of hundreds of meters, and the overall motion along the orbits is more chaotic. While X and Y components appear to oscillate around a constant value, the out-of-plane motion is subjected to an overall increasing trend, from negative mean position towards the orbital plane. It is also observed that in 0° and 120° oscillations are damped with time (planarization of the orbit), while in the 240° they become larger (Fig. 16).

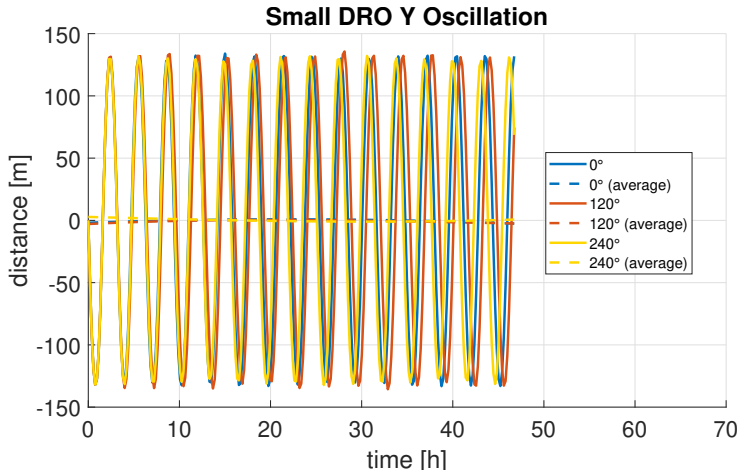

Fig. 14 Small DRO oscillations on Y axis.

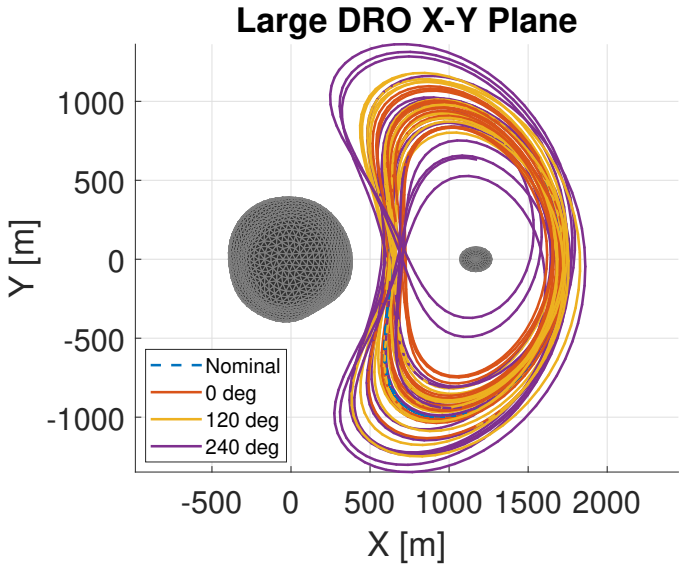

Fig. 15 Large DRO X-Y plane projection.

SPO orbits are characterized by periods in a ratio between 5:1 and 4:1 with respect to Didymain's rotation. As for DRO orbits, some are subjected to averaging effects, while others display resonance, depending on the distance from the asteroid's surface. In particular, considering the small SPO, the vertical component maintains a very stable position around an out-of-plane mean value, as shown in Fig. 17. Notice that vertical peaks of the motion around this orbit appear to get closer to the average value, suggesting a complete flattening of the orbit or, possibly, a very low frequency behavior in the

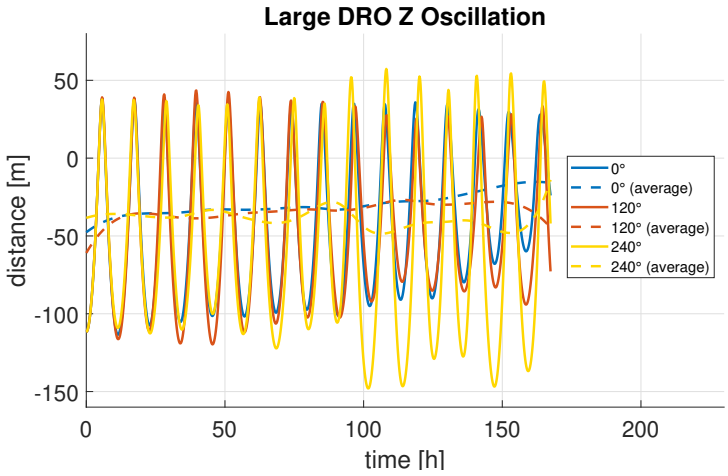

Fig. 16 Large DRO oscillations on Z axis.

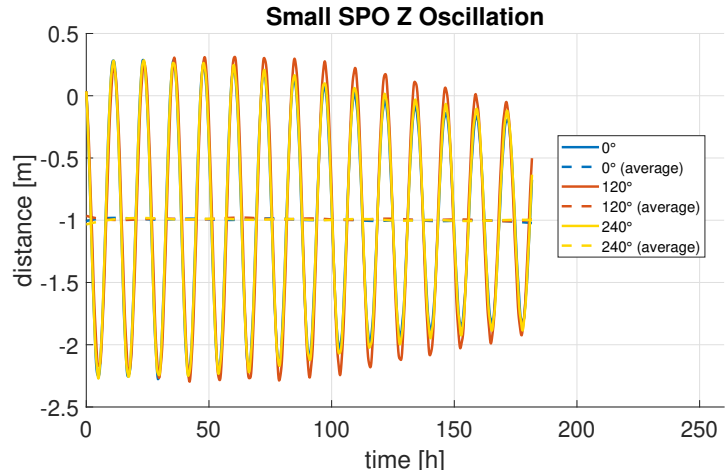

Fig. 17 Small SPO oscillations on Z axis.

out-of-plane motion. Regarding large SPO orbits, similar results in the vertical displacement are measured, however, the proximity of the trajectory to the asteroid's surface causes large perturbation in the in plane motion, moving the average X and Y positions back and forth of hundreds of meters. Fig. 18 shows this effect for the Y component (as the X component displays similar behavior). As a result, the orbits are pushed periodically towards the back and the front of main asteroid, with a relatively high frequency (see Fig. 19).

It is interesting to notice how the most perturbing effects (for both SPO and DRO orbits) are always related to a specific initial configuration of the main asteroid (240° for DROs, 120° for SPOs), proving that some effects from the equatorial ridge are present despite the high rotation, and

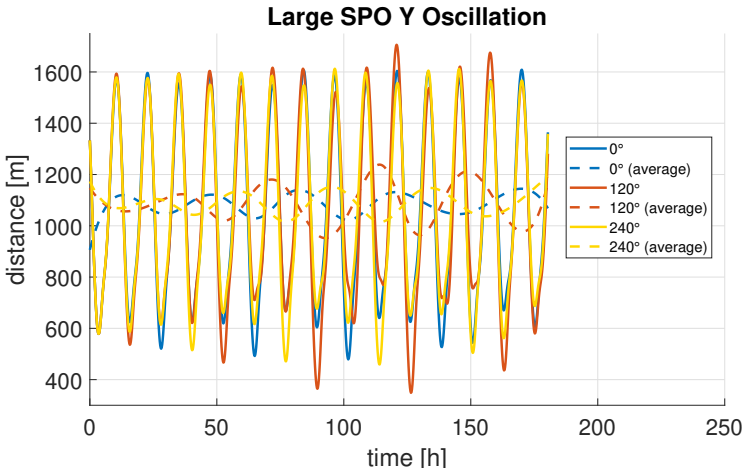

Fig. 18 Large SPO oscillations on Y axis.

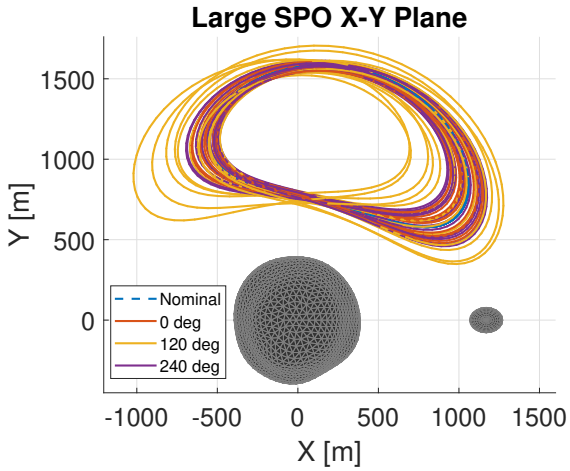

Fig. 19 Large SPO X-Y plane projection.

a complete averaging of gravity force cannot be attained.

VI. Conclusion

The paper addressed the topic of orbital dynamics around binary system of uneven celestial bodies, with specific application to the system 65803 Didymos. The study has been presented as a novel technique for periodic orbits search in this environment, and results of the process served for a classification of the trajectories in perturbed gravitational field, to highlight differences with respect to the classic point mass dynamics.

The dynamics around Didymos are modeled through a Shape-based Circular Restricted Three-Body Problem (SCR3BP) formulation, where point mass sources are replaced by shape-based models of asteroid's mass distribution. This was considered as a close-to-reality model of the dynamics as it refer to the most up-to-date information available on Didymos, although still relying on some dynamics assumptions. The algorithm to find periodic motion implements a novel strategy to investigate solutions in the SCR3BP, based on shape continuation of primaries. Correction is performed through multi-nodal correction and using a damped Levenberg-Marquardt algorithm. This allowed to deal with irregular gravity field without convergence or overshooting problems, at the cost of higher computational burden.

Orbital families found in the close-to-reality model have been analyzed and compared to the original CR3BP solutions, highlighting differences in shape, period, size and stability. The main result emerging from the study is the effect of the out-of-plane perturbation, which causes trajectory deformation as relevant as the overall orbital size increases. Such deviation is the confirmation that the CR3BP model can no longer be adopted in these type of systems, even for nearly spherical objects as the ones considered in the present work. In addition, significant differences in the size of smaller orbits have been detected, and related to energetic shifts of the equilibrium points in the system. Lyapunov orbits have shown unpredicted behavior and hint possible modifications in the orbital nature of such solutions due to the irregularities and asymmetries of the field. However, it is worth noting that CR3BP dynamics provide similar results in terms of period and stability properties. The subsequent introduction of the primary's rotation allowed to test the periodic solutions in a more realistic, non-synchronous system. The rotation caused some variations, with different effects depending on the specific orbit and its dimensions. However, for the orbits that maintained stability, the deviations appeared to be bounded, thus making the periodic trajectories, of the synchronous model, suitable for preliminary trajectory search.

The outcome of this work provide sets of families of periodic orbits in the close proximity of Didymos binary system and proves the effectiveness of the shape-based continuation method implemented. Orbital solutions discussed represents a step towards improved precision for irregular

gravity fields and realistic trajectory design. They can serve as basis for further and more detailed investigations, when more information on the binary system is available. Other features could be included in a further advancement step, to enhance the realism of the dynamics environment. These include eccentricity of the secondary's orbit and external perturbation sources (e.g. solar radiation pressure).

References

[1] Scheeres, D. J., "Dynamics about Uniformly Rotating Triaxial Ellipsoids: Applications to Asteroids," *Icarus*, Vol. 110, 1994, pp. 225–238. doi:10.1006/icar.1994.1118.

[2] Werner, R. A., and Scheeres, D. J., "Exterior Gravitation of a Polyhedron Derived and Compared with Harmonic and Mascon Gravitation Representations of Asteroid 4769 Castalia," *Celestial Mechanics and Dynamical Astronomy*, Vol. 65, 1997, pp. 313–344. doi:10.1007/bf00053511.

[3] Scheeres, D. J., Ostro, S. J., Hudson, R. S., DeJong, E. M., and Suzuki, S., "Dynamics of Orbits Close to Asteroid 4179 Toutatis," *Icarus*, Vol. 132, 1998, pp. 53–79. doi:10.1006/icar.1997.5870.

[4] Muller, P. M., and Sjogren, W. L., "Mascons: Lunar Mass Concentrations," *Science*, Vol. 161, No. 3842, 1968, pp. 680–684. doi:10.1126/science.161.3842.680.

[5] Colagrossi, A., Ferrari, F., Lavagna, M., and Howell, K., "Dynamical evolution about asteroids with high fidelity gravity field and perturbations modeling," *Advances in the Astronautical Sciences (Proceedings of the AIAA/AAS Astrodynamics Specialist Conference)*, Vol. 156, edited by J. Turner, G. Wawrzyniak, W. Cerven, and M. Majji, Univelt Inc., Napa, CA, USA, 2016, pp. 885–903.

[6] Ferrari, F., Tasora, A., Masarati, P., and Lavagna, M., "N-body gravitational and contact dynamics for asteroid aggregation," *Multibody System Dynamics*, Vol. 39, No. 1, 2017, pp. 3–20. doi:10.1007/s11044-016-9547-2.

[7] Geissler, P., Petit, J., Durda, D. D., et al., "Erosion and Ejecta Reaccretion on 243 Ida and Its Moon," *Icarus*, Vol. 120, No. 1, 1996, pp. 140 – 157. doi:http://dx.doi.org/10.1006/icar.1996.0042.

[8] Scheeres, D. J., Williams, B. G., and Miller, J. K., "Evaluation of the Dynamic Environment of an Asteroid: Applications to 433 Eros," *Journal of Guidance, Control, and Dynamics*, Vol. 23, No. 3, 2000, pp. 466–475. doi:10.2514/2.4552.

[9] Jiang, Y., "Equilibrium Points and Periodic Orbits in the Vicinity of Asteroids with an Application to 216 Kleopatra," *Earth, Moon, and Planets*, Vol. 115, No. 1, 2015, pp. 31–44. doi:10.1007/s11038-015-9464-z.

[10] Gabern, F., Koon, W. S., and Marsden, J. E., "Parking a Spacecraft Near an Asteroid Pair," *Journal of Guidance, Control, and Dynamics*, Vol. 29, 2006, pp. 544–553. doi:10.2514/1.15138.

[11] Bellerose, J., and Scheeres, D. J., "General Dynamics in the Restricted Full Three Body Problem," *Acta Astronautica*, Vol. 62, 2008, pp. 563–576. doi:10.1016/j.actaastro.2008.01.018.

[12] Bellerose, J., and Scheeres, D. J., "Restricted Full Three-Body Problem: Application to Binary System 1999 KW4," *Journal of Guidance, Control, and Dynamics*, Vol. 31, No. 1, 2008, pp. 162–171. doi:10.2514/1.30937.

[13] Chappaz, L., and Howell, K. C., "Exploration of bounded motion near binary systems comprised of small irregular bodies," *Celestial Mechanics and Dynamical Astronomy*, Vol. 123, 2015, pp. 123–149. doi:10.1007/s10569-015-9632-5.

[14] Pravec, P., Scheirich, P., Kušnirák, P., et al., "Photometric survey of binary near-Earth asteroids," *Icarus*, Vol. 181, 2006, pp. 63–93. doi:10.1016/j.icarus.2005.10.014.

[15] Cheng, A., Atchison, J., Kantsiper, B., et al., "Asteroid Impact and Deflection Assessment mission," *Acta Astronautica*, Vol. 115, No. Supplement C, 2015, pp. 262 – 269. doi:https://doi.org/10.1016/j.actaastro.2015.05.021.

[16] Cheng, A., Michel, P., Jutzi, M., et al., "Asteroid Impact & Deflection Assessment mission: Kinetic impactor," *Planetary and Space Science*, Vol. 121, No. Supplement C, 2016, pp. 27 – 35. doi:https://doi.org/10.1016/j.pss.2015.12.004.

[17] Michel, P., Cheng, A., Küppers, M., et al., "Science case for the Asteroid Impact Mission (AIM): A component of the Asteroid Impact & Deflection Assessment (AIDA) mission," *Advances in Space Research*, Vol. 57, No. 12, 2016, pp. 2529 – 2547. doi:https://doi.org/10.1016/j.asr.2016.03.031.

[18] Ferrari, F., and Lavagna, M., "Consolidated phase A design of Asteroid Impact Mission: MASCOT-2 landing on binary asteroid didymos," *Advances in the Astronautical Sciences*, Vol. 158, 2016, pp. 3759–3769.

[19] Tardivel, S., Lange, C., Ulamec, S., and Biele, J., "The deployment of Mascot-2 to Didymoon," *Advances in the Astronautical Sciences*, Vol. 158, 2016, pp. 3513–3533.

[20] Damme, F., Hussmann, H., and Oberst, J., "Spacecraft orbit lifetime within two binary near-Earth asteroid systems," *Planetary and Space Science*, Vol. 146, 2017, pp. 1–9. doi:10.1016/j.pss.2017.07.018.

[21] Dell'Elce, L., Baresi, N., Naidu, S., Benner, L., and Scheeres, D., "Numerical investigation of the dynamical environment of 65803 Didymos," *Advances in Space Research*, Vol. 59, No. 5, 2017, pp. 1304–1320. doi:10.1016/j.asr.2016.12.018.

[22] MacMillan, W. D., *The theory of the potential*, Dover, 1958, Chaps. 35–36, pp. 56–60. doi:10.1021/ed007p2530.

[23] Howell, K. C., "Three-Dimensional Periodic 'Halo' Orbits," *Celestial Mechanics*, Vol. 32, 1984, pp. 53–71. doi:10.1007/BF01358403.

[24] Lo, M. W., "Halo Orbit Generation Using the Center Manifold," *Proceedings of the AAS/AIAA Space Flight Mechanics Meeting*, Huntsville, AL, USA, 1997.

[25] Ferrari, F., "Non-Keplerian models for mission analysis scenarios about small solar system bodies," Ph.D. thesis, Italy, 2017.

[26] Gill, P. E., Murray, W., and Wright, M. H., *Practical optimization*, Academic press, 1981, Chap. 4, pp. 136–137. doi:10.1137/1025065.

[27] Fan, J. Y., and Yuan, Y. X., "On the quadratic convergence of the Levenberg-Marquardt method without nonsingularity assumption," *Computing*, Vol. 74, No. 1, 2005, pp. 23–39. doi:10.1007/s00607-004-0083-1.

[28] Howell, K. C., "Families of Orbits in the Vicinity of the Collinear Libration Points," *The Journal of the Astronautical Sciences*, Vol. 49, 2001, pp. 107–125. doi:10.2514/6.1998-4465.